ChemComm

COMMUNICATION

View Article Online
View Journal | View Issue

Cite this: *Chem. Commun.*, 2015, **51**, 9350

Received 9th March 2015,
Accepted 30th April 2015

DOI: 10.1039/c5cc02011e

www.rsc.org/chemcomm

The role of surface hydrolysis of ferricyanide anions in crystal growth of snowflake-shaped α-Fe_2O_3†

Zhong Liu,[ab] Chang-Yang Chiang,[b] Wu Li[a] and Wuzong Zhou*[b]

Selective adsorption and surface hydrolysis of $[Fe(CN)_6]^{3-}$ anions on α-Fe_2O_3 crystals was found to be a crucial process in the formation of a snowflake-like morphology, and the established mechanism is complementary to the classical theories of crystal growth.

Formation of high symmetric polyhedral morphologies of crystals can normally be explained using a kinetic approach of Bravais–Friedel–Donnay–Harker law, *i.e.* appearance of facets of a crystal is attributed to the slow growth rates along these directions. Another theory gives a thermodynamic approach: the equilibrium shape of a free crystal is the shape that minimizes its surface free energy. Both of these classical theories deal with the bonding energy of crystal structures without considering external effects, and therefore, cannot explain the formation mechanisms of many unusual crystal morphologies, *e.g.* polyhedra of polycrystalline particles of calcite and MOFs,[1] complicated snowflake-shaped hematite (α-Fe_2O_3).[2] The anisotropy of the crystal structure of hematite cannot justify the only active crystal growth directions of six equivalent zone axes, parallel to the (*ab*) plane of the hexagonal unit cell.

Hematite, as the most stable iron oxide under ambient conditions, is a good candidate for application in many fields, including catalysis, gas sensors, lithium battery, magnetic materials production, electromagnetic devices and pigments, *etc.*[3] In recent years, it has been found that these applications are greatly affected by the microstructures and morphologies of the crystals.[4] 'Snowflake' α-Fe_2O_3 with hyperbranches has been investigated because of their large surface areas and unique hierarchical structures.[5] However, the formation mechanism of these morphologies is yet to be studied.

Herein, we report our recent re-synthesis of 'snowflake' α-Fe_2O_3 crystals *via* a hydrolysis process of $[Fe(CN)_6]^{3-}$. The growth directions of $\langle 11\bar{2}0\rangle$ instead of commonly reported $\langle 10\bar{1}0\rangle$ are detected from selected area electron diffraction (SAED) patterns and high resolution transmission electron microscopic (HRTEM) images. The growth direction was found to be governed by highly selective surface adsorption followed by on-site hydrolysis of ferricyanide anions. Addition of octylamine in the synthetic solution led to a change in the favourite growth directions from $\langle 11\bar{2}0\rangle$ to $\langle 10\bar{1}0\rangle$ and induced a morphology evolution from 'snowflake' to 'starfish', 'flower' and finally to hexagonal plate, offering further support to the newly established mechanism.

'Snowflake' α-Fe_2O_3 particles were synthesized according to the reported method.[2] 1.52 mmol $K_3Fe(CN)_6$ were dissolved in 40 mL deionized water. The solution was subsequently sealed in a 50 mL autoclave, and maintained at 180 °C for 20 h, followed by cooling down to room temperature gradually. Almost all the particles in the red precipitate have a snowflake-like shape (Fig. S1a, b, ESI†). The XRD pattern of the product shows a single phase of α-Fe_2O_3 with all the diffraction peaks indexed onto the hexagonal unit cell with a = 5.0356 and c = 13.7489 Å (Fig. S2a, ESI†).

A TEM image of a typical 'snowflake' particle is shown in Fig. 1(a), revealing more microstructural details. Although the constructed hyperbranched microstructure of the particle looks quite complicated, the corresponding SAED pattern (Fig. 1b) indicates that the whole particle can be regarded as a single crystal, and the viewing direction perpendicular to the face of the 'snowflake' is along the [0001] zone axis of α-Fe_2O_3. In other words, all the branches and sub-branches in the particle are linked through a crystalline connection. Comparable examples are mesoporous single crystals of metal oxides.[6] It can also be confirmed by HRTEM images that the crystal growth directions are the six $\langle 11\bar{2}0\rangle$ zone axes (Fig. 1d, e). The whole particle is quite flat with a smooth (0001) surface, while the diameter of the 'snowflake' particles is about 10 μm, which is much larger than the particle sizes of other specimens as shown in Fig. S1, ESI.† It again implies that the growth along the $\langle 11\bar{2}0\rangle$ directions is fast. If the diffusion rates and attachment behaviour of the building units, such as Fe^{3+} and OH^-, to various crystal

[a] *Key Laboratory of Salt Lake Resources and Chemistry, Qinghai Institute of Salt Lakes, Chinese Academy of Sciences, Xining 810008, China*
[b] *EaStChem, School of Chemistry, University of St Andrews, St Andrews, KY16 9ST, UK. E-mail: wzhou@st-andrews.ac.uk*

† Electronic supplementary information (ESI) available: More SEM, TEM, HRTEM images, XRD patterns and XPS spectra of α-Fe_2O_3 specimens. See DOI: 10.1039/c5cc02011e

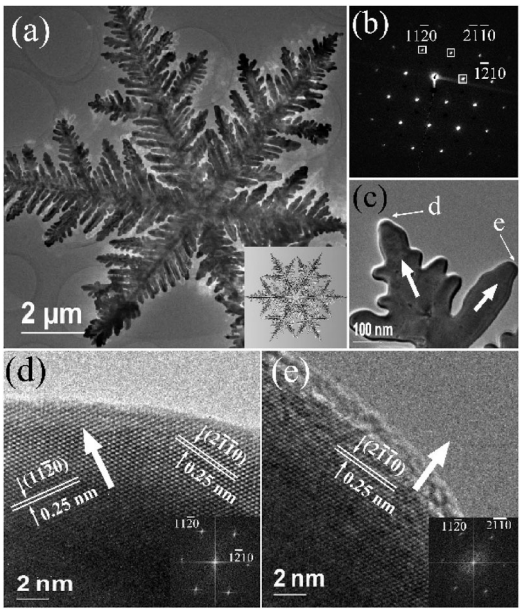

Fig. 1 (a) TEM image of a typical snowflake-like particle of α-Fe_2O_3. The inset is a photo of a real snowflake for comparison. (b) The corresponding SAED pattern. (c) An enlarged TEM image of a tip. (d) and (e) HRTEM images from the tip areas marked 'd' and 'e' in (c), respectively. The arrows indicate the crystal growth directions. The insets are the corresponding FFT patterns.

surfaces are similar, such highly selective directions of crystal growth cannot be explained based on the crystallographic anisotropy of α-Fe_2O_3.

We assume, in the initial stage, some nuclei of α-Fe_2O_3 form in the solution of $K_3Fe(CN)_6$ *via* the following hydrolysis process.

$$[Fe(CN)_6]^{3-} \leftrightarrow [Fe(H_2O)_x]^{3+} \rightarrow FeOOH/Fe(OH)_3 \rightarrow \alpha\text{-}Fe_2O_3.$$

SEM and HRTEM investigations of time-dependant specimens (Fig. S3, ESI†) indicate that the processes of nucleation and growth of spherical crystallites are very slow. Further crystal growth of the branches is much faster. The latter process relies on attachment of precursor ions/molecules on the crystal surface. Since the dissociation of $[Fe(CN)_6]^{3-}$ in water is extremely low with the dissociation constant, $K_d = 1.0 \times 10^{-42}$, there are almost no Fe^{3+} free cations in the solution. On the other hand, hydrolysis of $[Fe(CN)_6]^{3-}$ results in a reduction of pH value from 7.27 to 6.76 (see Table S1, ESI†) and, therefore, the concentration of OH^- anions is also very low. The principal precursor ions in the solution are $[Fe(CN)_6]^{3-}$. These ferricyanide anions contain six lone pairs of electrons on the outer surface, which can bond on the crystal surface if the latter contains some exposed positive charged sites or Lewis acidic sites.

Under the hydrothermal synthetic conditions, the surface of metal oxide crystals is normally terminated with hydroxyl groups. Close examination of the terminal atomic planes on the principal facets of α-Fe_2O_3, such as the {10$\bar{1}$0}, {11$\bar{2}$0}, and {0001} planes, has been previously performed and their electronic structures calculated.[7] The charge of the hydroxyl groups depends on the local configuration, *i.e.* the number of Fe coordination. If a hydroxyl group is coordinated by only one Fe cation, it is negatively charged, designated site I or $OH^{0.5-}$. A doubly coordinated hydroxyl group is neutralized, designated site II or OH^0, while that in a triple coordination is positively charged, designated site III or $OH^{0.5+}$. The {0001} surfaces of hematite contain only doubly coordinated hydroxyl groups with a density of 13.7 nm^{-2}, which are neutral and inactive in the surface adsorption of ferricyanide anions. The {10$\bar{1}$0} surfaces have both singly and doubly coordinated hydroxyls (5.8 nm^{-2} and 2.9 nm^{-2}, respectively) and are, therefore, overall negatively charged, which is also inactive for bonding with the ferricyanide anions. The {11$\bar{2}$0} surfaces contain all the three types of co-ordinations (5.0 nm^{-2} for each type of sites). The positively charged $OH^{0.5+}$ in the triply coordinated hydroxyl groups can act as Lewis acidic sites, offering a chance to bond with $[Fe(CN)_6]^{3-}$. This is probably the most important factor of the selective crystal growth along the ⟨11$\bar{2}$0⟩ directions.

Fig. 2(a) shows a top view of the (11$\bar{2}$0) surface. The hydroxyl groups having different Fe coordinations (sites I, II and III) are indicated with the triply coordinated oxygen highlighted by a pink shadow. Fig. 2(b) is a profile view of the (11$\bar{2}$0) surface *via* rotation of the model in Fig. 2(a) around the *Z* axis for 90°. H atoms on site III are shown. When a $[Fe(CN)_6]^{3-}$ anion is adsorbed on the (11$\bar{2}$0) surface as shown in the middle of Fig. 2,

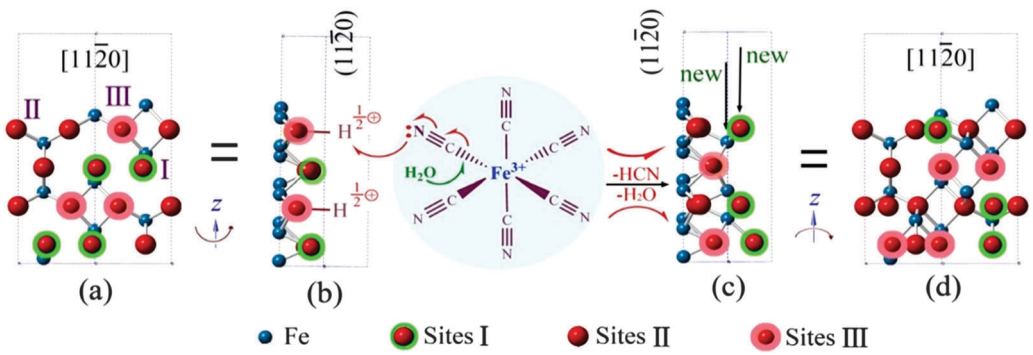

Fig. 2 Schematic drawing of the surface adsorption of a $[Fe(CN)_6]^{3-}$ anion to the positively charged triply coordinated hydroxyl group on the (11$\bar{2}$0) surface and its surface hydrolysis into α-Fe_2O_3. (a) and (b) Top view and profile view with H on site III of the (11$\bar{2}$0) surface. (c) and (d) Profile view and top view of the surface with a newly deposited layer of α-Fe_2O_3.

bonding with $OH^{0.5+}$, partial electron transfer from a CN^- ligand to the crystal surface weakens the Fe–C bond, enhancing the surface hydrolysis of the $[Fe(CN)_6]^{3-}$ anion. All the CN^- ligands would eventually leave Fe on the surface sites followed by dehydrogenation and dehydration, leading to deposition of α-Fe_2O_3 as shown in Fig. 2(c and d). The original triply coordinated oxygen atoms become four coordinated and the singly coordinated sites become triply coordinated, *i.e.* new sites III. The process can go on. Since such a surface hydrolysis only takes place on the $\{11\bar{2}0\}$ surfaces, and the growth on the $\{10\bar{1}0\}$ and {0001} surfaces is greatly depressed, the final morphology of the crystals becomes two dimensional thin snowflake-like. When the hydrolysis is not completed, a small amount of CN^- might remain on the crystal surface, as detected by XPS (Fig. S4a, ESI†).

When octylamine was added into the solution with a concentration of 0.12 mol L^{-1}, the morphology of product changed from 'snowflake' to 'starfish' with six arms, while the particle size decreases to about 3 μm (Fig. S1c, d, ESI†). Although six primary branches were also developed in each crystal, the details of the hyperbranched structure, as seen in a TEM image in Fig. 3(a), is different from 'snowflake' crystals. First, the secondary branches are close to each other, leaving no room for growth of the tertiary branches. Secondly, the thickness of the primary branches along [0001] increases significantly. Therefore, the particles are no longer thin and flat. Finally and most importantly, a careful analysis of SAED and HRTEM revealed that the principal crystal growth directions have been shifted from $\{11\bar{2}0\}$ to $\{10\bar{1}0\}$, as presented in Fig. 3(a,b).

With a further increase of the concentration of octylamine to 0.24 mol L^{-1} and 0.36 mol L^{-1}, the hyperbranched structure completely disappears. The centres of the particles grow out, showing a hexagonal flower-like morphology. The diameters of the particles further decrease to 1 μm and below (Fig. S1e–h, ESI†). Fig. 3(c,d) shows TEM and HRTEM images of a typical flower-like particle. Analysis of both the corresponding SAED pattern and *d*-spacings in the HRTEM image confirms that the principal growth directions are along the $\langle 10\bar{1}0\rangle$ zone axes.

The effects of octylamine can be understood in two aspects. The overall reaction of hydrolysis of $[Fe(CN)_6]^{3-}$ can be written as

$$2[Fe(CN)_6]^{3-} + 3H_2O \leftrightarrow \alpha\text{-}Fe_2O_3 + 6H^+ + 12CN^-.$$

As a weak alkali capping agent, octylamine can enhance the above reaction. Consequently, the concentration of $[Fe(CN)_6]^{3-}$ anions in the solution would be reduced. On the other hand, octylamine ($pK_b = 3.35$) is a relatively strong alkaline compound than ferricyanide anions ($pK_b = 4.86$).[8] Therefore, octylamine can directly bond with the $OH^{0.5+}$ on site III of the $\{11\bar{2}0\}$ surfaces, blocking these surfaces. The surface hydrolysis of ferricyanide anions as described in Fig. 2 is greatly suppressed. XPS of flower-like crystals shows a small N 1 s peak at a binding energy of 399.47 eV (Fig. S4a, ESI†), which has a significantly higher intensity than that from snowflake crystals (Fig. S4b, ESI†) and can be attributed to the surface adsorption of octylamine.[9]

Another effect of amine on the surface hydroxyl configuration is from the alkaline property of the solution, as seen in Table S1, ESI.† The $OH^{0.5+}$ groups on the $\{11\bar{2}0\}$ surfaces would be more or less neutralized. When NaOH was added instead of octylamine, no 'snowflake' were produced, and both the particle size and morphology changed with the concentration of NaOH.

The transformation of $[Fe(CN)_6]^{3-}$ to Fe_2O_3 cannot be a direct process. It may be achieved *via* formation of series intermediate ions, *e.g.* $[Fe(H_2O)_x(CN)_{6-x}]^{x+3-}$ (x = 1 to 6). The charge of the Fe-containing ions changes from 3− to 3+ step-by-step. When site III is no longer available for adsorption of negatively charged ions, site I with $OH^{0.5-}$ becomes the active site to attract positively charged ions. In other words, Fe-containing cations would go to the $\{11\bar{2}0\}$ and $\{10\bar{1}0\}$ surfaces. Bearing in mind the former is blocked by octylamine, the most active surface for crystal growth would be the latter. This proposed mechanism explains why the crystal growth directions shifted from the $\langle 11\bar{2}0\rangle$ to $\langle 10\bar{1}0\rangle$ zone axes when octylamine was added.

When the concentration of octylamine was increased to 0.48 and 0.60 mol L^{-1}, the pH value of the solution increased further. The charge difference of the hydroxyl groups on all the surfaces became less obvious. The hydrolysis of $[Fe(CN)_6]^{3-}$ only took place in the solution. The crystal growth turned to a normal process, and the morphology of the produced particles gradually changed to hexagonal plates as shown in Fig. S1(i–l), ESI.† The average diameters of the particles reduced to 500 nm to 400 nm, respectively, while their thickness increased significantly. TEM and HRTEM images in Fig. S5, ESI† confirm such a crystal morphology.

In summary, from the formation of snowflake-shaped α-Fe_2O_3, we learnt a new phenomenon of crystal growth, interaction of precursor ions with the crystal surface produces the building

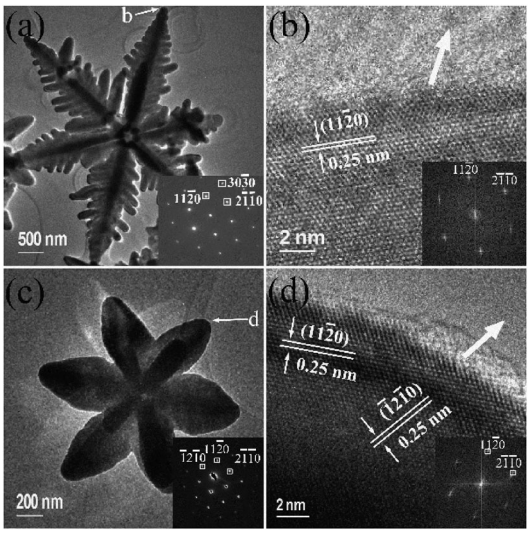

Fig. 3 (a) TEM image of a typical 'starfish' particle from the sample prepared with 0.12 mol L^{-1} octylamine. The inset is the corresponding SAED pattern. (b) HRTEM image of a tip area, marked by 'b', of the particle in (a). (c) TEM image of a 'flower' α-Fe_2O_3 particle from the sample prepared with 0.24 mol L^{-1} octylamine. The inset is the corresponding SAED pattern. (d) HRTEM image from a tip area, marked by 'd', of the particle in (c). The insets in (b) and (d) are the FFT pattern from the whole areas. The arrows in (b) and (d) indicate the crystal growth directions of $[10\bar{1}0]$.

units for crystals on selective sites, leading to specific growth directions. Low dimensional and complicated morphologies can form in free crystals with no templates or surface modification with ligands. This mechanism may be used to explain formation of many novel crystal morphologies.

This work was supported by the NSFC (No. 51302280), NSF of Qinghai (2014-ZJ-936Q), and Young Scholar Project of Qinghai Institute of Salt Lakes, Chinese Academy of Sciences. WZ thanks EPSRC for financial support to the Electron Microscopy Laboratory (EP/F019580/1).

Notes and references

1 A. Ritchie, M. Watson, R. Turnbull, Z. Lu, M. Telfer, J. Gano, K. Self, H. F. Greer and W. Z. Zhou, *CrystEngComm*, 2013, **15**, 10266; C. M. Zheng, H. F. Greer, C.-Y. Chiang and W. Z. Zhou, *CrystEngComm*, 2014, **16**, 1064.
2 Z. Liu, B. L. Lv, D. Wu, Y. Zhu and Y. H. Sun, *CrystEngComm*, 2012, **14**, 4074.
3 N. D. Carbonare, V. Cristino, S. Berardi, S. Carli, R. Argazzi, S. Caramori, L. Meda, A. Tacca and C. A. Bignozzi, *ChemPhysChem*, 2014, **15**, 1164; X. L. Gou, G. X. Wang, J. Park, H. Liu and J. Yang, *Nanotechnology*, 2008, **19**, 125606; Z. Y. Wang, D. Y. Luan, S. Madhavi, C. M. Li and X. W. Lou, *Chem. Commun.*, 2011, **47**, 8061; C. Z. Wu, P. Yin, X. Zhu, C. Z. OuYang and Y. Xie, *J. Phys. Chem. B*, 2006, **110**, 17806; Y. Kim, J. H. Pee, J. H. Chang, K. Choi, K. J. Kim and D. Y. Jung, *Chem. Lett.*, 2009, **38**, 842.
4 B. L. Lv, Z. Y. Liu, H. Tian, Y. Xu, D. Wu and Y. H. Sun, *Adv. Funct. Mater.*, 2010, **20**, 3987.
5 M. H. Cao, T. F. Liu, S. Gao, G. B. Sun, X. L. Wu, C. W. Hu and Z. L. Wang, *Angew. Chem., Int. Ed.*, 2005, **44**, 4197.
6 W. B. Yue and W. Z. Zhou, *Prog. Nat. Sci.*, 2008, **18**, 1329.
7 R. M. Cornell and U. Schwertman, *The Iron Oxides: Stucture, Properties, Reaction, Occurences and Use*, Wiley VCH GmbH&Co. KGaA, 2nd edn, 2003, p. 222; V. Barron and J. Torrent, *J. Colloid Interface Sci.*, 1996, **177**, 407; C. H. Rochester and S. A. Topham, *J. Chem. Soc., Faraday Trans. 1*, 1979, **75**, 1073.
8 Z. Wan, W. L. Luan and S. T. Tu, *J. Phys. Chem. C*, 2011, **115**, 1569.
9 Z. Liu, B. L. Lv, D. Wu, Y. H. Sun and Y. Xu, *Eur. J. Inorg. Chem.*, 2012, 4076.